Structural and magnetic properties of $Fe_{76}P_5(Si_{0.3}B_{0.5}C_{0.2})_{19}$ amorphous alloy

G.C. Lavorato [a,b], G. Fiore [b], P. Tiberto [c], M. Baricco [b], H. Sirkin [a], J.A. Moya [d,*]

[a] INTECIN (FIUBA-CONICET), Paseo Colón 850, Capital Federal, Argentina
[b] Dipartimento di Chimica IFM and NIS, Università di Torino, Torino, Italy
[c] INRIM, Electromagnetism Division, Torino, Italy
[d] GIM – IESIING, Universidad Católica de Salta, INTECIN (UBA-CONICET), Argentina

ABSTRACT

Recently, bulk amorphous alloys were produced in the Fe–B–Si–P–C system with high glass forming ability, excellent magnetic properties and the advantage of containing no expensive glass-forming elements, such as Ga, Y, Cr or Nb, having, therefore, a good perspective of commercial applications. In the present work, the $Fe_{76}P_5(Si_{0.3}B_{0.5}C_{0.2})_{19}$ amorphous alloy prepared by two quenching techniques has been studied. Amorphous ribbons of about 40 μm thick were obtained by planar-flow casting together with cylinders having 1 and 2 mm diameter produced by copper mold injection casting. All the samples appear fully amorphous after X-ray diffraction analysis. A comprehensive set of thermal data (glass, crystallization, melting and liquidus temperatures) were obtained as well as a description of the melting and solidification processes. Mechanical microhardness tests showed that the samples have a hardness of 9.7 ± 0.3 GPa. Good soft-magnetic properties were obtained, including a high magnetization of 1.44 T and a low coercivity (4.5 A/m for ribbons and 7.5 A/m in the case of 1 mm rod samples, both in as-cast state). Thermomagnetic studies showed a Curie temperature around 665 K and the precipitation of new magnetic phases upon temperatures of 1000 K. Furthermore, the frequency dependence of magnetic losses at a fixed peak induction was studied. The results suggest the occurrence of a fine magnetic domain structure in bulk samples. The good soft magnetic properties of the bulk metallic glass obtained by copper mold casting for this particular Fe-based composition suggests possible applications in transformer cores, inductive sensors and other devices.

© 2011 Elsevier B.V. All rights reserved.

1. Introduction

Ferromagnetic metallic glasses sheets have shown an interesting combination of magnetic, mechanical and chemical properties. These materials have been produced since 1967 [1], but their thickness was limited to the range of few micrometers because of the high cooling rate required during solidification to hinder crystallization (about 10^6 K/s). Nowadays, the use of ferromagnetic amorphous alloys in efficient transformer cores is becoming more widespread, as they are the magnetically softest commercially available materials. However, cores made of thin sheets (usually about 40 μm thick) present some difficulties associated with the lack of self-sustainability. In addition, great core sizes are necessary, due to the gap between sheets that, added to after-annealing brittleness and sensitivity to mechanical stresses [2], make desirable the development of bulk amorphous alloys.

The first ferromagnetic bulk metallic glass alloy was obtained in 1995 [3] using a copper mold, with cooling rates lower than 100 K/s.

Since then, much research effort has been devoted to enhance the saturation magnetization and to reduce the coercive field of ferromagnetic bulk metallic glasses. Such a goal is not an easy task, as tailoring the alloy composition with the goal of improving magnetic properties must preserve the requirements of a high glass forming ability (GFA).

Recently, bulk amorphous alloys with Fe–B–Si–P–C composition, containing no other metallic element than iron usually necessary to reach an adequate GFA, have been developed by Inoue et al. [4,5]. In this case, the saturation magnetization is not reduced by the addition of glass forming elements and reaches a value of 1.44 T. In particular, the developed alloys are based on the well-known Fe–B–Si system, where B has been partially replaced by non-metallic P and C, allowing the formation of amorphous rods with diameter up to 3 mm.

This paper is focused on the study of the alloy $Fe_{76}P_5(B_{0.5}C_{0.3}Si_{0.2})_{19}$ whose composition was found to be the optimum in the mentioned system [4]. Combining measurements of thermal stability and magnetic properties, including magnetic losses and temperature dependence of magnetization, a full picture on glass formation and possible applications was obtained.

* Corresponding author. Tel.: +54 387 4268587.
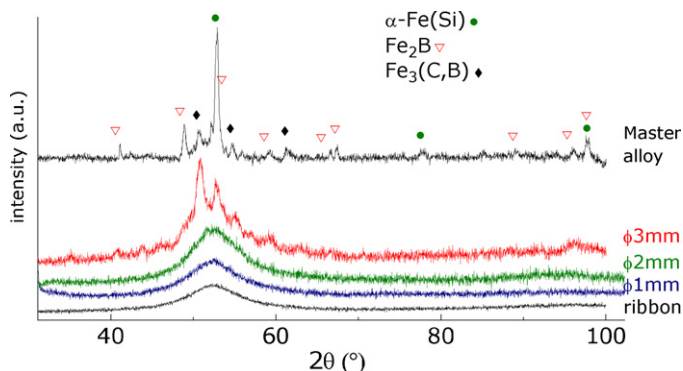 E-mail address: jmoya.fi.uba@gmail.com (J.A. Moya).

Fig. 1. XRD patterns of master alloy, ribbons and rods samples with different diameters.

2. Experimental

A master alloy of composition $Fe_{76}P_5(Si_{0.3}B_{0.5}C_{0.2})_{19}$ was prepared using Fe, Si and C pure elements (>99.9%) and Fe–B and Fe–P (>98.9%) ferroalloys in an arc melting furnace under Ar atmosphere. In order to optimize the C content and avoid mass losses during the melting process, a Fe–C alloy was previously prepared and its composition was evaluated by a calorimetric analysis of melting. The master alloy was remelted at least five times to get chemical homogeneity and the mass loss resulted to be less than 0.2%. Then, 40 μm thick and 4 mm width ribbons were produced by planar-flow casting, and cylindrical rods of 1, 2 and 3 mm diameter were obtained by injection copper mold casting technique.

X-ray diffraction (XRD) was employed to study the structure of the samples (Philips PW1830 diffractometer with Co-Kα radiation, λ = 1.7897 Å). Differential scanning calorimetry (DSC) studies were conducted in a Perkin Elmer Diamond – DSC device at a heating rate of 0.33 K/s and high temperature measurements were performed in a Setaram HTDSC at a heating rate of 0.083 K/s.

The microstructure of the obtained samples was examined with an optical microscope and with a scanning electron microscope (SEM-LeicaStereoscan 420). In addition, energy dispersive spectroscopy (EDS) was employed to verify the chemical composition of the samples. The density of bulk samples was measured by the Archimedes' technique using deionized water and, in the case of ribbon samples, the density was estimated by numerous size-weight measurements. Hardness measurements were performed using a Buehler Vickers microhardness tester at an applied load of 300 g for 15 s.

Magnetization vs. temperature experiments (at an applied field of 80 kA/m and a heating rate of 0.083 K/s), and saturation magnetization measurements (at a maximum field of 800 kA/m) were carried out in a Lake Shore 7400 Vibrating Sample Magnetometer (VSM). Inductive hysteresis loops and magnetic losses in the material were measured using a digital feedback wattmeter under sinusoidal induction waveform [6] in the frequency range from 1 to 500 Hz at a fixed magnetic induction of 0.6 T [7].

3. Results and discussion

X-ray diffraction patterns of master alloy, ribbon and bulk samples are shown in Fig. 1. Three different phases can be identified in the master alloy: an α-Fe(Si) solid solution, together with Fe_2B and $Fe_3(C,B)$ compounds. No crystalline phases were detected in as-quenched ribbon, 1 and 2 mm bulk samples. The 3 mm diameter bulk sample presents some crystalline peaks superimposed to the amorphous halo. These peaks correspond to the same phases present in the master crystalline alloy, as it can be noticed when comparing the two spectra.

A back-scattering SEM image of the master alloy is shown in Fig. 2. It reveals a primary phase that corresponds to Fe_2B compound and an eutectic mixture, likely formed by the α-Fe(Si) solid solution and the $Fe_3(C,B)$, as detected by XRD. In the case of bulk samples, back-scattering SEM images of the 1 mm diameter rod does not reveal any contrast and confirms the presence of a single amorphous phase, as shown in Fig. 3(a). In the case of 2 mm diameter sample, microcrystalline phases are observed on the surface of the rod (Fig. 3(b) and (c)). Some defects along the surface of the mold could have promoted the formation of nucleation sites and the successive growth of crystalline phases, but it is noteworthy
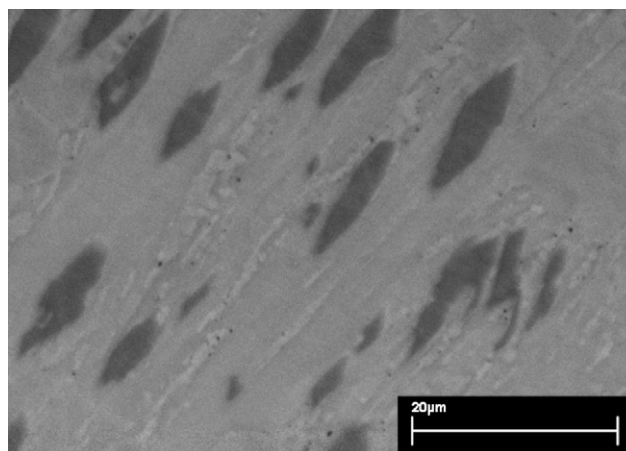

Fig. 2. Back-scattering SEM image of the master alloy.

that the core of the rod resulted fully amorphous in all samples. The optical micrograph of the 3 mm diameter sample (Fig. 3(d)) reveals an amorphous matrix (as observed by XRD) with some crystallites distributed in the inner region of the cylinder.

DSC traces of the ribbon and of 1 and 2 mm diameter rods are shown in Fig. 4(a). It can be seen that all samples show a similar behavior with the crystallization occurring in a single exothermic signal. The values of Curie, glass transition and crystallization temperatures (Tc, Tg, Tx, respectively) were determined and the results are reported in Table 1. The results confirm the formation of a glassy phase in the three different samples. However, the 2 mm rod presents a significantly lower heat of crystallization (ΔH_X) in comparison to the other samples; this fact is probably due to a partial crystallization during the casting process, as reported in Fig. 3(b). The sample shows a supercooled liquid region ($\Delta T_x = T_x - T_g$) of about 50 K, in good agreement with results obtained previously [4]. The HTDSC traces of the melting and solidification of the master alloy are reported in Fig. 4(b). The melting and liquidus temperatures (T_m and T_l, respectively) remain constant during continuous heating as well as during continuous cooling, indicating that no significant undercooling phenomenon occurs. The melting reaction (T_m = 1232 K) involves a mixture of phases presumably with the presence of the Fe_2B compound and is followed by a barely visible liquidus point at higher temperature. The DSC trace of solidification reveals a small exothermic peak due to the liquidus (T_l = 1422 K) followed by a broad shoulder and by partially overlapped exothermic reactions. This result suggests the formation of a complex structure far from eutectic. It is worth noting that compositions most favorable for glass formation are usually close to eutectics, even if, for multicomponent alloys, high GFA off-eutectic compositions have been reported. Combining the results obtained with the thermal analysis, the value of γ parameter, which is taken as an indicator of the GFA of the alloy [8], can be calculated. It turns out equal to 0.37, confirming the high GFA for this alloy composition.

Bulk amorphous samples showed a Vickers hardness value of about 9.7 ± 0.3 GPa, which was obtained after averaging several measurements, in good agreement with the high strength measured by compressive test [4]. Density was determined to be 7100 ± 50 kg/m^3 for bulk samples and 7000 ± 100 kg/m^3 for ribbons.

The magnetic hysteresis loops for the studied alloys are shown in Fig. 5. The differences in the susceptibility are due to the presence of a non-negligible demagnetizing field in the case of cylinders samples. All samples show the same value of saturation magnetization ($M_s \sim 1.44 \pm 0.02$ T) listed in Table 1. Inductive measurements at 1 Hz revealed a coercive field value, H_c, of 4.5, 7.5 and 20.5 A/m

Table 1
DSC data, magnetic properties and mechanical hardness, H_v, for $Fe_{76}P_5(C_{0.2}B_{0.5}Si_{0.3})_{19}$ as-cast ribbon and bulk amorphous alloys: T_c, T_g and T_x: Curie, glass and crystallization temperatures.; ΔH_x, heat of crystallization; Ms, saturation magnetization; H_c, coercive field; P/c, magnetic losses per cycle (50 Hz and 0.6 T).

	T_c (K)	T_g (K)	T_x (K)	ΔH_x (J/g)	M_s (T)	H_c (A/m)	H_v (GPa)	P/c (mJ/kg)
Ribbon	666	755	810	−92	1.44	4.5	–	2.13
1 mm rod	668	760	810	−91	1.44	7.5	9.7	3.14
2 mm rod	668	760	811	−84	1.42	20.5	9.8	15.21
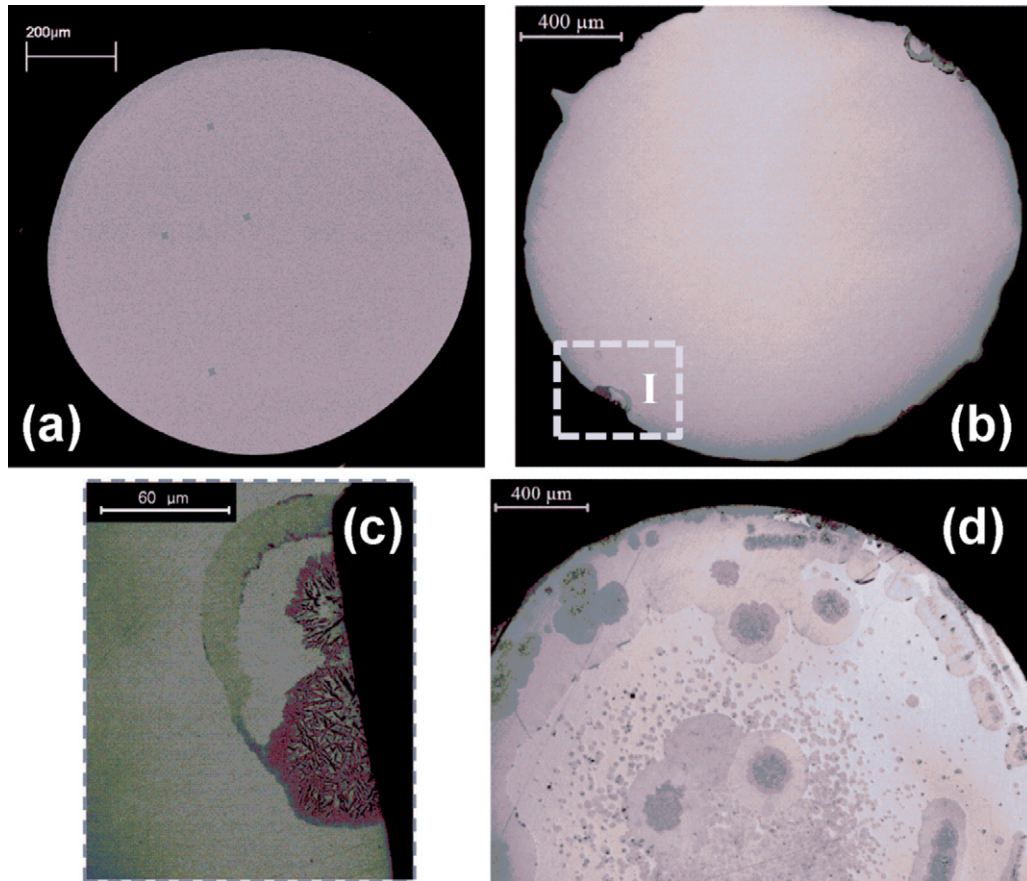
Fig. 3. (a) Backscattered electron SEM image of 1 mm diameter rod sample. (b) Optical micrograph of the 2 mm diameter rod sample. (c) Detail I. (d) Optical micrograph of the 3 mm diameter rod sample.
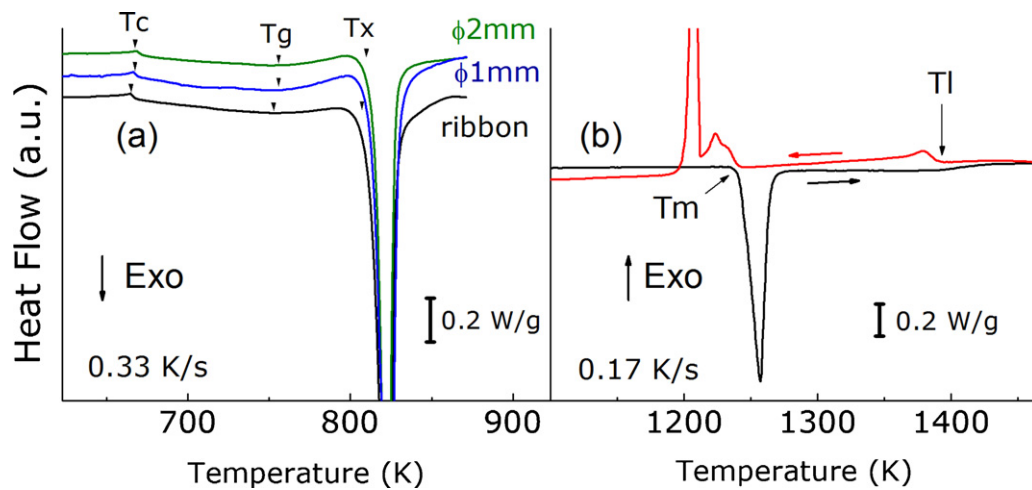
Fig. 4. (a) Low temperature DSC curve of amorphous samples. (b) High temperature DSC curve of the master alloy.
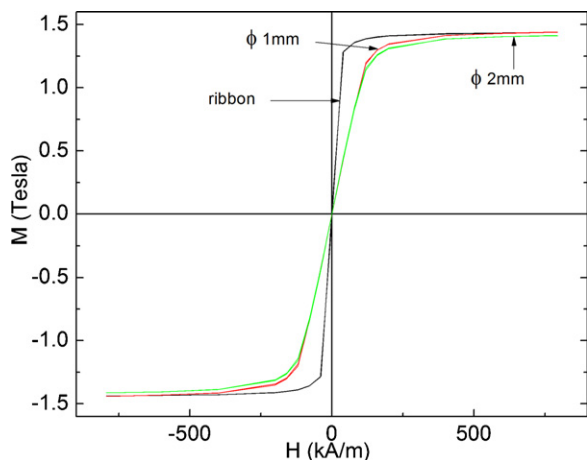
Fig. 5. VSM hysteresis loops of ribbon and rod samples.

for ribbon, 1 mm and 2 mm bulk samples, respectively. Higher coercive fields are expected in as-cast bulk metallic glasses with respect to ribbons, as greater residual stresses are supposed to be present due to a high difference in cooling rates between the surface and the inner region of the cylinder [9,10]. In addition, bulk alloys are more prone to structural inhomogeneities (such as micro pores) that could act as pinning centers for the domain walls movements, leading to a higher coercivity value.

The frequency dependence of magnetic losses per cycle between 1 and 500 Hz is reported in Fig. 6. A loss separation model [11,12] was employed for a better comprehension of the origin of magnetic losses and of the magnetic structure of the material. In this model total losses can be decomposed into hysteresis, classical and excess contributions according to:

$$P_{tot} = P_{hyst} + P_{class} + P_{exc} \tag{1}$$

Hysteresis losses (P_{hyst}) are related to domains wall movement that must overcome the energy barriers formed by the pinning centers. This process is essentially not affected by frequency as jumps are in the order of 10^{-8} or 10^{-9} s and the magnetization time, $1/f$, is much smaller. Classical losses (P_{class}) depend on geometrical factors and electrical conductivity of the material and they scale directly with frequency, while the excess losses (P_{exc}) are related to the domain
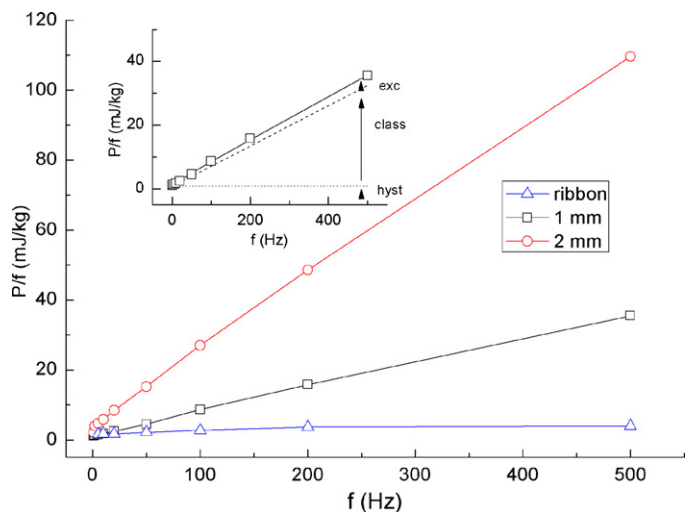

Fig. 6. Magnetic losses per cycle with frequency. Inset: loss separation for 1 mm rod sample. Magnetic losses contributions are indicated.
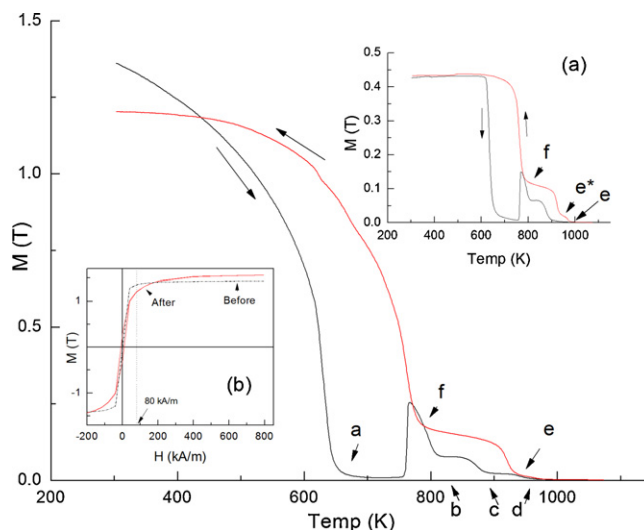

Fig. 7. Thermomagnetic behavior of ribbon and 1 mm rod sample, in inset (a). Inset (b): Hysteresis loops of the ribbon sample before and after the thermomagnetic experiment.

structure. According to the model, the measured data can be fitted using the following expression:

$$P_{tot} = k_0 + k_1 f + k_2 f^{1/2} \tag{2}$$

As shown in the inset of Fig. 6, the fitting results for bulk samples reveal that classical losses are the main contribution to total losses, as expected due to considerably high thickness of the sample. The analysis of magnetic losses contributions indicates that, in the studied frequency range, the excess losses always represent less than 35% of total losses, suggesting the presence of a fine domains structure. Moreover, when frequencies are greater than 10 Hz, the geometrical factors and induced eddy currents in the material play an important role by increasing the classical losses component. These results should be carefully taken into account when designing a highly efficient magnetic device.

Magnetic losses obtained at $f = 50$ Hz T taken at a maximum induction of 0.6 T (see Table 1) can be compared to those of a grain oriented Fe–Si (≈ 7 mJ/kg) or Metglas® 2605 amorphous alloy (≈ 2 mJ/kg) measured at 60 Hz and 0.7 T [7].

The thermomagnetic behavior of the ribbon and 1 mm rod samples (inset) are shown in Fig. 7. The heating curve shows that the Curie temperature (T_c) of the amorphous phase is around 665 K ("a" in Fig. 7) in agreement with the DSC results. This first stage of the thermomagnetic behavior might be useful in order to determine the maximum working temperature as well as the better condition for heat treatment under magnetic field. After the crystallization of the amorphous phase, three new ferromagnetic contributions can be detected having T_c of about 820 K, 895 K and 965 K ("b", "c" and "d" points respectively). During cooling, only two ferromagnetic phases could be observed with $T_c \sim 935$ and ~ 820 K ("e" and "f" points respectively). This result suggests that the ferromagnetic phase with $T_c = 895$ K observed on heating is metastable and, possibly, corresponds to orthorhombic Fe$_3$B [13]. Finally, when the system is cooled down to room temperature, the observed magnetization is smaller than the initial one. This result can be ascribed to the presence of a magnetocrystalline anisotropy value higher than that of a fully amorphous phase (see Fig. 7 inset (b)). The highest T_c on cooling (point "e") corresponds to the α-Fe(Si) phase, with about 15.5% at. Si [14] while the T_c at 800 K (point "f") may be related to Fe$_2$B boride, whose T_c is reported in a temperature range of 785–793 K [15,16].

Magnetization behavior as function of temperature in bulk samples is rather the same except that: (i) the initial and final magnetizations of the thermomagnetic curves are equal due to the low value of magnetization reached in samples with high demagnetized factor; (ii) during cooling a new ferromagnetic phase is clearly observed at high temperatures. This phase is almost unnoticeable but also present in the thermomagnetic behavior of the ribbons, has a T_c of about 985 K, namely "e*" in the inset graph (a).

4. Conclusions

A comprehensive study of structural and magnetic properties of $Fe_{76}P_5(Si_{0.3}B_{0.5}C_{0.2})_{19}$ amorphous alloys prepared in ribbon (40 μm thick) and cylinder (1 and 2 mm diameter) forms was reported. A complete set of thermal data was presented with the obtained values of glass transition, crystallization, melting and liquidus temperatures. The γ parameter of 0.37 suggests a good glass forming ability of the alloy while HTDSC studies reveal that this is an off-eutectic composition alloy.

Thermomagnetic experiments indicate that the Curie temperature of the amorphous sample is around 665 K. Continuous heating up to 1000 K revealed the formation of three magnetic phases: Fe_3B (tetragonal and orthorhombic) and α-Fe(Si) with about 15.5 at.% Si. Then, a full picture of the temperature range for possible use is provided, and adequate annealing temperatures in induced magnetic field can be established for technological applications.

Saturation magnetization and coercitive field of about 4.5, 7.5 and 20.5 A/m were measured for ribbon, 1 mm and 2 mm rod, respectively and results are in good agreement with results obtained by Chang et al. in as-cast samples, as well as, our obtained value of average Vickers hardness of 9.7 ± 0.3 GPa. Furthermore density was determined for bulk and ribbons samples in 7100 ± 50 kg/m^3 and 7000 ± 100 kg/m^3, respectively.

The analysis of the magnetic losses performed up to 500 Hz indicates a good fine domain structure in the bulk samples, being the geometrical factor the primary cause of the losses in frequencies above 10 Hz (classical losses). This has been observed also in the rod 2 mm thick (magnetic losses increase about 3 times). The knowledge of these data is essential to design high-performance magnetic devices.

In conclusion, the magnetic losses obtained for this material were found to be very competitive in relation to those of traditional materials at frequencies close to 60 Hz, being between 2 and 3 times less than grain-oriented Fe–Si. The description of the effect of frequency on magnetic losses, with the analysis of the extensive and intensive contributions, is essential when designing high performance magnetic devices. These values indicate that the material has a potential industrial interest and can be used in the future in transformer cores, inductive sensors and other electrical devices.

References

[1] P. Duwez, J. Appl. Phys. 38 (1967) 4096.
[2] T.D. Shen, R.B. Schwarz, Appl. Phys. Lett. 75 (1999) 49.
[3] A. Inoue, J.S. Gook, Mater. Trans. JIM 36 (1995) 1180–1183.
[4] C. Chang, T. Kubota, A. Makino, A. Inoue, J. Alloy Compd. 473 (2009) 368–372.
[5] A. Makino, T. Kubota, C. Chang, M. Makabe, A. Inoue, J. Magn. Magn. Mater. 320 (2008) 2499–2503.
[6] G. Bertotti, E. Ferrara, F. Fiorillo, M. Pasquale, J. Appl. Phys. 73 (1993) 5375.
[7] F. Fiorillo, A. Novikov, IEEE Trans. Magn. 26 (1990) 2559–2561.
[8] Z. Lu, Acta Mater. 50 (2002) 3501–3512.
[9] M. Stoica, S. Roth, J. Eckert, L. Schultz, M. Baro, J. Magn. Magn. Mater. 290–291 (2005) 1480–1482.
[10] E. Ustundag, B. Clausen, J.C. Hanan, M.A.M. Bourke, A. Winholtz, A. Pekers, MRS Proc. 554 (2011) 431–436.
[11] G. Bertotti, IEEE Trans. Magn. 24 (1988) 621–630.
[12] P. Tiberto, R. Piccin, N. Lupu, H. Chiriac, M. Baricco, J. Alloy Compd. 483 (2009) 608–612.
[13] Y. Kong, F. Li, Phys. Rev. B 56 (1997) 3153–3158.
[14] R. Bozorth, Ferromagnetism, IEEE Press, Piscataway N.J, 1993.
[15] R. Coehoorn, D.B. de Mooij, J.P.W.B. Duchateau, K.H.J. Buschow, J. Phys. Colloques 49 (1988), C8-669–C8-670.
[16] T. Tarnoczi, I. Nagy, C. Hargitai, M. Hosso, Trans. Magn., IEEE 14 (1978) 1025–1027.